PNAS RESEARCH ARTICLE | GENETICS

An inherited life-threatening arrhythmia model established by screening randomly mutagenized mice

Yuta Okabe[a], Nobuyuki Murakoshi[a,1], Nagomi Kurebayashi[b,1], Hana Inoue[c], Yoko Ito[a], Takashi Murayama[b], Chika Miyoshi[d], Hiromasa Funato[d], Koichiro Ishii[b], Dongzhu Xu[a], Kazuko Tajiri[a], Rujie Qin[a], Kazuhiro Aonuma[a], Yoshiko Murakata[a], Zonghu Song[a], Shigeharu Wakana[e,f], Utako Yokoyama[c], Takashi Sakurai[b], Kazutaka Aonuma[a], Masaki Ieda[g], and Masashi Yanagisawa[d,1]

Contributed by Masashi Yanagisawa; received October 27, 2022; accepted February 27, 2024; reviewed by Michael Rubart and Héctor H. Valdivia

Inherited arrhythmia syndromes (IASs) can cause life-threatening arrhythmias and are responsible for a significant proportion of sudden cardiac deaths (SCDs). Despite progress in the development of devices to prevent SCDs, the precise molecular mechanisms that induce detrimental arrhythmias remain to be fully investigated, and more effective therapies are desirable. In the present study, we screened a large-scale randomly mutagenized mouse library by electrocardiography to establish a disease model of IASs and consequently found one pedigree that exhibited spontaneous ventricular arrhythmias (VAs) followed by SCD within 1 y after birth. Genetic analysis successfully revealed a missense mutation (p.I4093V) of the ryanodine receptor 2 gene to be a cause of the arrhythmia. We found an age-related increase in arrhythmia frequency accompanied by cardiomegaly and decreased ventricular contractility in the *Ryr2*$^{I4093V/+}$ mice. Ca^{2+} signaling analysis and a ryanodine binding assay indicated that the mutant ryanodine receptor 2 had a gain-of-function phenotype and enhanced Ca^{2+} sensitivity. Using this model, we detected the significant suppression of VA following flecainide or dantrolene treatment. Collectively, we established an inherited life-threatening arrhythmia mouse model from an electrocardiogram-based screen of randomly mutagenized mice. The present IAS model may prove feasible for use in investigating the mechanisms of SCD and assessing therapies.

inherited arrhythmia syndrome | forward genetics | animal model | ryanodine receptor 2 | catecholaminergic polymorphic ventricular tachycardia

Sudden cardiac death (SCD) is a significant public health problem accounting for approximately 4.25 million deaths per year worldwide (1). Although myocardial infarction and cardiomyopathies are major causes of SCD, inherited arrhythmia syndromes (IASs) are the leading cause in adolescents (2). IASs include several genetic heart disorders, mainly primary arrhythmia syndromes, also called ion channelopathies. The majority of genes causative of IASs encode components of ion channels or regulatory proteins that modify ion channel functions, mutations of which cause abnormalities in action potential (AP) and, subsequently, induce life-threatening arrhythmias (3). Genetic testing for IASs is recommended because of the high probability of detecting the causative genes in some diseases (4).

Recent progress in sequencing technologies and biological analyses has provided novel insights into the pathogenic mechanisms of IASs (5–7). However, molecular mechanisms underlying the spontaneous onset of arrhythmia and subsequent SCD remain to be fully elucidated. Furthermore, disease-specific treatments, such as molecular-targeting drugs, have not yet been developed, although implantable cardioverter-defibrillators have been established as effective therapies for secondary prevention in IAS patients with aborted cardiac arrest (7, 8). To overcome the challenges of studying SCD in inherited arrhythmia diseases, a suitable animal model that recapitulates the human disease is desirable.

Phenotype-driven forward genetics—a research strategy that provides an estimation of the identity of causative genes from the heritability of the objective phenotype—has been successfully applied in several fields (9–11). This method has the advantage of not being constrained by a specific working hypothesis and therefore has the potential to lead to highly novel discoveries (12). We previously identified novel sleep- and wakefulness-regulating genes via an electroencephalogram/electromyogram-based screen of a large-scale chemical-mutagen-induced mutagenized mouse library (13). Here, we screened a mutagenized mouse library using electrocardiography (ECG) to identify mice with the target phenotype: hereditary arrhythmia. We thus established a mouse pedigree harboring a novel ryanodine receptor 2 gene (*Ryr2*) missense mutation that exhibited bidirectional ventricular tachycardia (BVT) spontaneously leading to SCD as a model of IASs.

Significance

Sudden cardiac death (SCD) is a major public health issue. Inherited arrhythmias account for a large portion of SCDs in adolescents. We established a mouse pedigree that exhibits severe inherited arrhythmias with SCD after electrocardiographically screening a large-scale randomly mutagenized mouse library. The present model harbors a *Ryr2* missense mutation that is regarded as a gain-of-function mutation with high Ca^{2+} sensitivity that induces spontaneous Ca^{2+} leak at the subcellular level. Spontaneous ventricular arrhythmias leading to SCDs were observed, and flecainide and dantrolene were effective at suppressing arrhythmias in this model, which were similar characteristics of catecholaminergic polymorphic ventricular tachycardia. The present model can be applied to investigate the pathophysiological mechanisms of SCD and to assess therapeutic strategies, especially drugs.

Author contributions: N.M. and M.Y. designed research; Y.O., N.M., N.K., H.I., Y.I., T.M., C.M., H.F., K.I., D.X., K.T., R.Q., Kazuhiro Aonuma, Y.M., Z.S., S.W., U.Y., T.S., Kazutaka Aonuma, and M.I. performed research; Y.O., N.M., N.K., and T.M. analyzed data; and Y.O., N.M., N.K., and M.Y. wrote the paper.

Reviewers: M.R., Indiana University School of Medicine; and H.H.V., University of Wisconsin-Madison.

The authors declare no competing interest.

[1]To whom correspondence may be addressed. Email: yanagisawa.masa.fu@u.tsukuba.ac.jp; n.murakoshi@md.tsukuba.ac.jp; or nagomik@juntendo.ac.jp.

This article contains supporting information online at https://www.pnas.org/lookup/suppl/doi:10.1073/pnas.2218204121/-/DCSupplemental.

Published April 15, 2024.

Results

Spontaneous Ventricular Arrhythmia Mouse Pedigree Harbors *Ryr2* Missense Mutation. To elucidate the unrevealed genetic mutations behind the inherited arrhythmia, we screened a randomly mutagenized F_1 mouse library generated from male C57BL/6J (B6J) mice harboring point mutations induced by ethylnitrosourea (ENU) and female C57BL/6N (B6N) mice (G_0) (*SI Appendix*, Fig. S1). ECG screening of more than 7,000 F_1 mice identified one mouse with spontaneous BVT. The pedigree of this founder showed distinct heritability for the arrhythmia phenotype. The arrhythmic mice of this pedigree manifested various types of spontaneous ventricular arrhythmias (VAs), i.e., BVT, polymorphic ventricular tachycardia (PVT), and premature ventricular complex (PVC) bigeminy, contrary to the wild-type littermates, which had only sinus rhythm without VA (Fig. 1*A*). Linkage analysis of the B6J×B6N N_2 generation from the arrhythmic founder produced a single LOD score peak on chromosome 13, upstream of D13SNP30 (rs3722313, chr13: 41538155) (Fig. 1 *B* and *C*). Whole-exome sequencing in four mice with spontaneous BVT and two wild-type mice (B6J and B6N) and direct DNA sequencing of the phenotype-positive and -negative mouse genomes identified a heterozygous single-nucleotide substitution in the *Ryr2* gene (c.12277A>G) (Fig. 1 *D* and *E*). The identified mutation resulted in an amino acid substitution from isoleucine to valine at position 4093.

Ryr2 encodes ryanodine receptor 2 (RyR2), a cardiac isoform of the ryanodine receptor, which is a Ca^{2+} channel located in the membrane of the sarcoplasmic reticulum (SR). The release of stored Ca^{2+} through RyR2 is initiated by an increase in intracellular Ca^{2+} via L-type Ca^{2+} channels, called Ca^{2+}-induced Ca^{2+} release (CICR) (14). RyR2 is a homotetramer, with each monomer comprising the large cytoplasmic domains and the channel domains connected by the central domain (15), where the I4093V

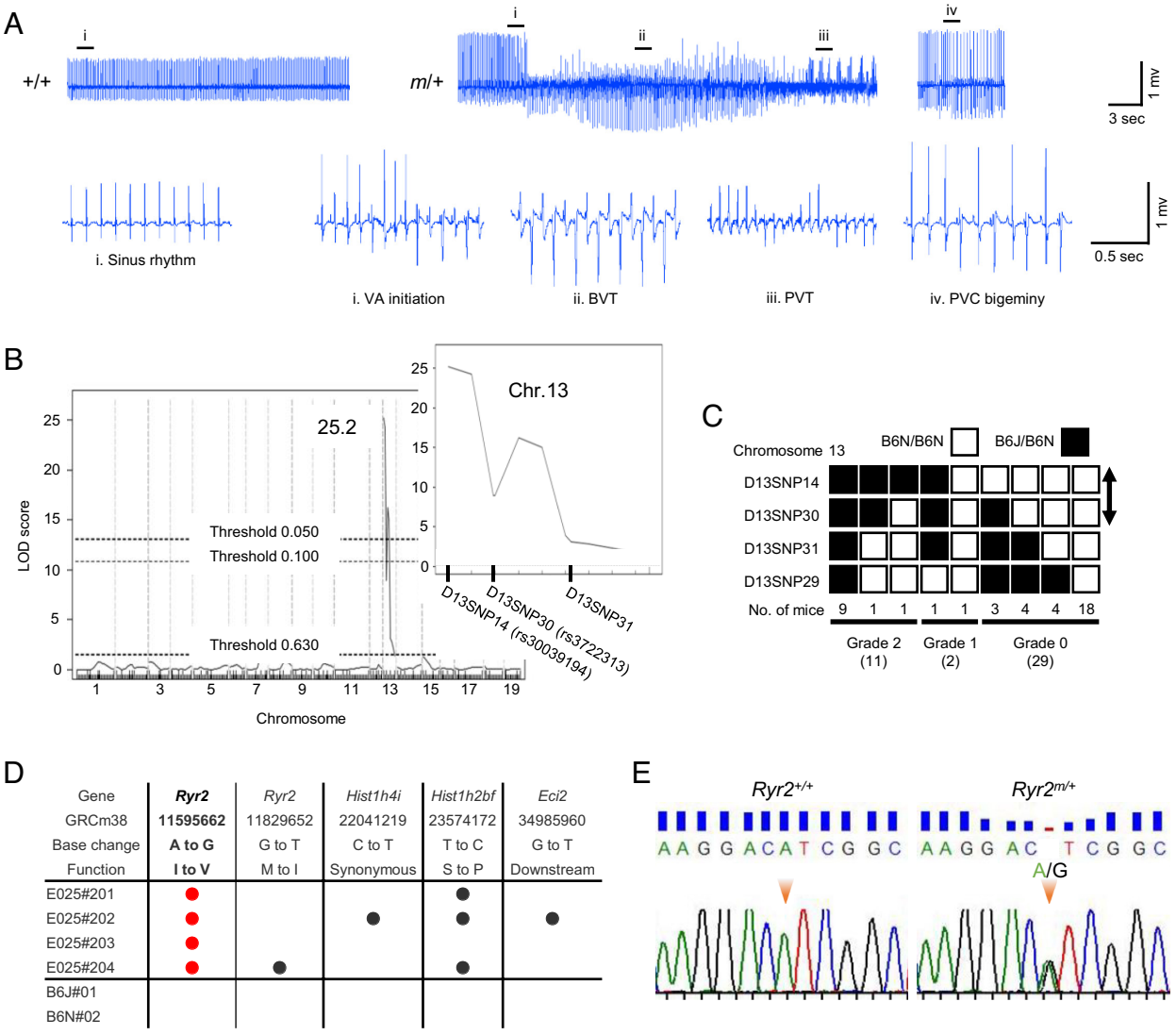

Fig. 1. Forward-genetics approach identifies one ventricular-arrhythmia pedigree harboring a *Ryr2* missense mutation. (*A*) Representative ECGs of +/+ and *m*/+ mice. The *Left* panel shows +/+ mouse ECG with regular sinus rhythm (i). The *Right* panel shows *m*/+ mouse ECG with VA initiation (i), BVT (ii), PVT (iii), and PVC bigeminy (iv). (*B*) Quantitative trait locus (QTL) analysis of VT pedigree (n = 42) for the frequency of VAs. The graph shows a logarithm of the odds (LOD) score peak located upstream of D13SNP30 in chromosome 13. (*C*) Haplotype analysis of VT pedigree by VA frequency. Semiquantitative parameters of VA frequency: Grade 0, no arrhythmia; Grade 1, only a single arrhythmia event (single, nonconsecutive PVC and/or RR interval irregularity); Grade 2, PVC bigeminy and/or VT. (*D*) Exome sequencing in four mice from VT pedigree (E025#201–#204) and two wild-type mice (B6J and B6N) within LOD score peak region. (*E*) Direct DNA sequencing of the *Ryr2* gene in $Ryr2^{+/+}$ and $Ryr2^{m/+}$ mice.

mutation resides (*SI Appendix*, Fig. S2). The amino acids surrounding the identified isoleucine mutation in RyR2 are highly conserved phylogenetically (*SI Appendix*, Fig. S3). The pathogenic mutations of RyR2 have been reported to be associated with the IASs catecholaminergic polymorphic ventricular tachycardia (CPVT) (16) and idiopathic ventricular fibrillation (17).

Arrhythmia Characteristics and Electrocardiographic Findings in *Ryr2*$^{I4093V/+}$ Mice. We conducted surface ECG and continuous 24-h ECG to investigate the VA frequency and ECG parameters of *Ryr2*$^{I4093V/+}$ mice. Interestingly, the mutant mice showed a clear increase in VA frequency with age (Fig. 2*A*). At the age of 2 mo, the *Ryr2*$^{I4093V/+}$ mice rarely showed VA under basal conditions, similar to the wild type; however, low-dose epinephrine (1 mg/kg) injections easily evoked VA, but only in the *Ryr2*$^{I4093V/+}$ mice (Fig. 2*B*). Continuous ECG recordings revealed that the dark–light cycle did not affect the VA frequency of *Ryr2*$^{I4093V/+}$ mice at 4 to 5 mo old (Fig. 2*C*). The mean heart rate (HR) also showed no significant difference between the two groups (Fig. 2*D*). Furthermore, we found that ECG morphology was similarly affected by age. The study group was divided into young (Yng) mice (2 to 3 mo old) and old (Old) mice (5 to 7 mo old) to clarify age-related alterations in ECG parameters. In young mice, these parameters were not significantly different between *Ryr2*$^{+/+}$ and *Ryr2*$^{I4093V/+}$ groups. In contrast, QRS and QTc durations were significantly prolonged in old *Ryr2*$^{I4093V/+}$ mice compared with those in old *Ryr2*$^{+/+}$ mice (Fig. 2 *E*–*G*). Comparably, the R wave amplitude was higher in old *Ryr2*$^{I4093V/+}$ mice than in old *Ryr2*$^{+/+}$ mice, but not significantly (Fig. 2 *E* and *H*). These results indicate that the *Ryr2*$^{I4093V/+}$ mice developed catecholaminergic arrhythmogenicity at a younger age, similar to CPVT patients. Furthermore, older *Ryr2*$^{I4093V/+}$ mice were more vulnerable to VAs accompanied by QRS complex and T wave alterations.

Increased Incidence of Sudden Death in *Ryr2*$^{I4093V/+}$ Mice. We hypothesized that *Ryr2*$^{I4093V/+}$ mice had a poorer prognosis than their wild-type littermates, as this is characteristic of CPVT (18). We prospectively assessed the incidence of sudden death

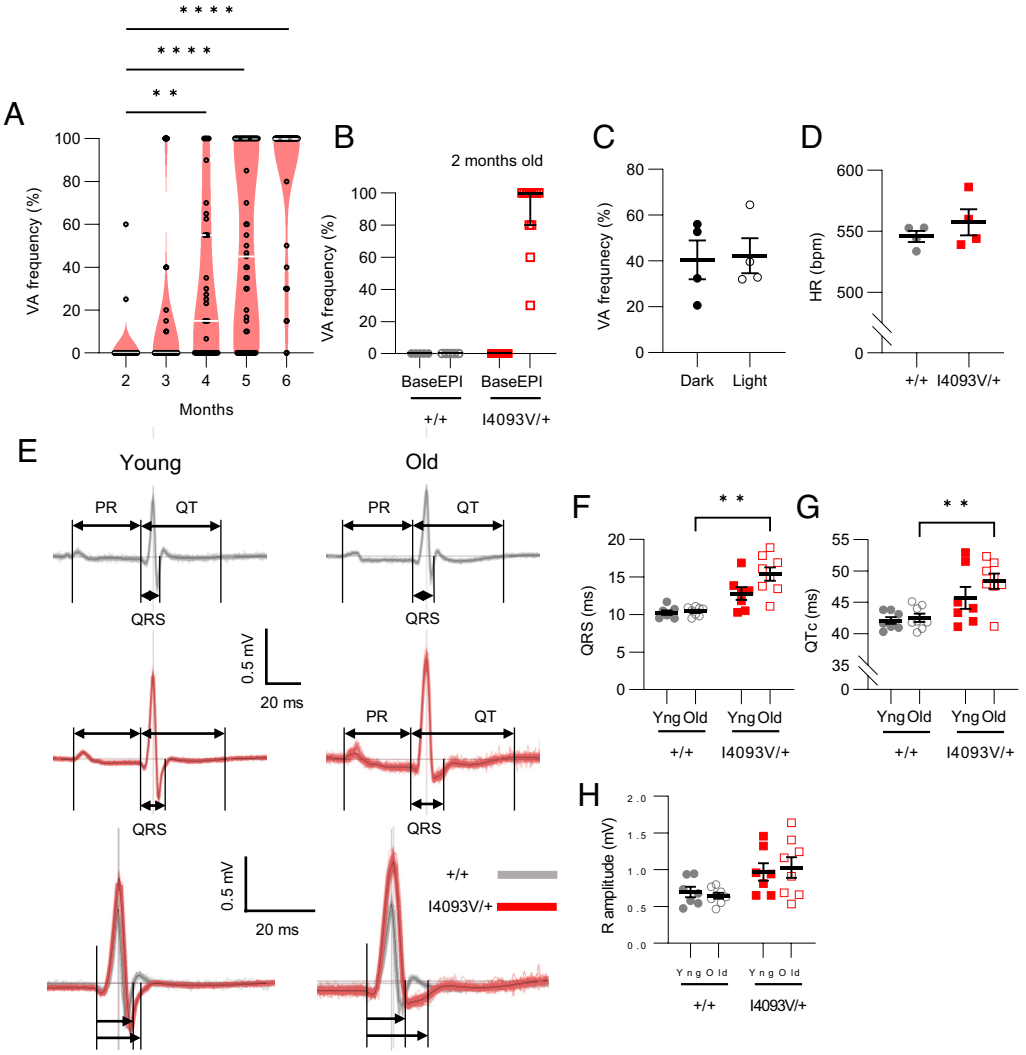

Fig. 2. *Ryr2*$^{I4093V/+}$ mice show age-related VA susceptibility with electrocardiographic morphological changes. (*A*) VA frequency by age in *Ryr2*$^{I4093V/+}$ mice (n = 40, 55, 35, 59, and 46 at 2, 3, 4, 5, and 6 mo old, respectively). Data are shown in violin plots. White lines and white dotted lines indicate the medians and the quartiles, respectively. $^{**}P < 0.01$ and $^{****}P < 0.0001$ by the Kruskal–Wallis test with Dunn's post hoc test. (*B*) VA frequency before (Base) and after epinephrine (EPI) administration in *Ryr2*$^{+/+}$ (n = 5) and *Ryr2*$^{I4093V/+}$ (n = 12) mice at 2 mo of age. (*C*) VA frequency and ventricular tachycardia (VT) rate comparison of the dark–light cycle in 24-h ECG of *Ryr2*$^{I4093V/+}$ mice (n = 4). Means were compared by the paired *t*-test. (*D*) Mean HR during 24-h ECG recording in *Ryr2*$^{+/+}$ and *Ryr2*$^{I4093V/+}$ mice (n = 4 in each group). Means were compared by the *t*-test. (*E*) Exemplar signal-averaged ECG traces using QRS maximum for the alignment. Mice aged 2 to 3 and 5 to 7 mo old were defined as young (Yng) and old (Old), respectively. The lowest row shows superimposed QRS complexes at expanded time scales. (*F*–*H*) QRS (*F*) and QTc (*G*) duration and R wave amplitude (*H*) comparing young (n = 7) and old (n = 8) *Ryr2*$^{+/+}$ mice and young (n = 7) and old (n = 8) *Ryr2*$^{I4093V/+}$ mice. $^{**}P < 0.01$ by Welch's ANOVA with Dunnett's T3 post hoc test.

in *Ryr2*$^{I4093V/+}$ mice and their wild-type littermates. A greater incidence of sudden death was observed in *Ryr2*$^{I4093V/+}$ mice (13/13; 100%) than in wild-type mice (2/29; 6.9%) ($P < 0.0001$) (Fig. 3*A*). All deaths of *Ryr2*$^{I4093V/+}$ mice occurred when they were 6 to 12 mo of age. To observe the onset of arrhythmia followed by SCD, we examined a 7-mo-old *Ryr2*$^{I4093V/+}$ mouse challenged with epinephrine (2 mg/kg). After epinephrine administration, incessant VT collapsed into PVT and the mouse died 10 min after the injection (*SI Appendix*, Fig. S4). Because of a previous report describing that RyR2 mutation is associated with seizures (19), electroencephalography of *Ryr2*$^{I4093V/+}$ mice was performed to examine the possibility that central nervous system disorders, including epilepsy, were involved in the death in *Ryr2*$^{I4093V/+}$ mice. The screening of their records for 3 consecutive days showed no abnormal waveforms associated with epilepsy (*SI Appendix*, Fig. S5). Altogether, these results demonstrated that the mutant mice recapitulated the phenotype of SCD from severe IASs.

Cardiac Structural and Histological Phenotypes of *Ryr2*$^{I4093V/+}$ Mice. We measured the heart weight and performed echocardiography and histological analysis in *Ryr2*$^{I4093V/+}$ mice to determine the physiological influence of the I4093V RyR2 mutation. We also compared the parameters of the two age groups mentioned above. Old *Ryr2*$^{I4093V/+}$ mice showed evident cardiac enlargement compared with old *Ryr2*$^{+/+}$ mice (Fig. 3*B*). Heart weight was significantly greater in old *Ryr2*$^{I4093V/+}$ mice than in their age-matched wild-type littermates (Fig. 3*C*), and lung weight showed a similar trend (Fig. 3*D*). Furthermore, old *Ryr2*$^{I4093V/+}$ mice had a significantly lower left ventricular (LV) ejection fraction (LVEF) and larger LV posterior wall diameter and mass than young *Ryr2*$^{I4093V/+}$ mice and old wild-type mice (Fig. 3 *E* and *F* and *SI Appendix*, Table S1). Cardiomyocyte dimensions were quantified and showed a significant increase in the old *Ryr2*$^{I4093V/+}$ group compared with those in the young *Ryr2*$^{I4093V/+}$ or wild-type group (Fig. 3 *G* and *H*), indicating that myocyte hypertrophy significantly contributed to the ventricular remodeling in *Ryr2*$^{I4093V/+}$ heart. We also examined the proportion of the fibrotic area in the LV axial sections from the old mouse groups and found no significant increase in fibrosis in *Ryr2*$^{I4093V/+}$ mice compared with that in wild-type mice (Fig. 3*I* and *SI Appendix*, Fig. S6). Taken together, these findings indicate that *Ryr2*$^{I4093V/+}$ hearts exhibited ventricular hypertrophy and dysfunction associated with aging, similar to the ECG findings.

Abnormal Ca^{2+} Handling in Isolated *Ryr2*$^{I4093V/+}$ Cardiomyocytes. We examined the Ca^{2+}-signaling properties of cardiomyocytes derived from *Ryr2*$^{I4093V/+}$ mice and their

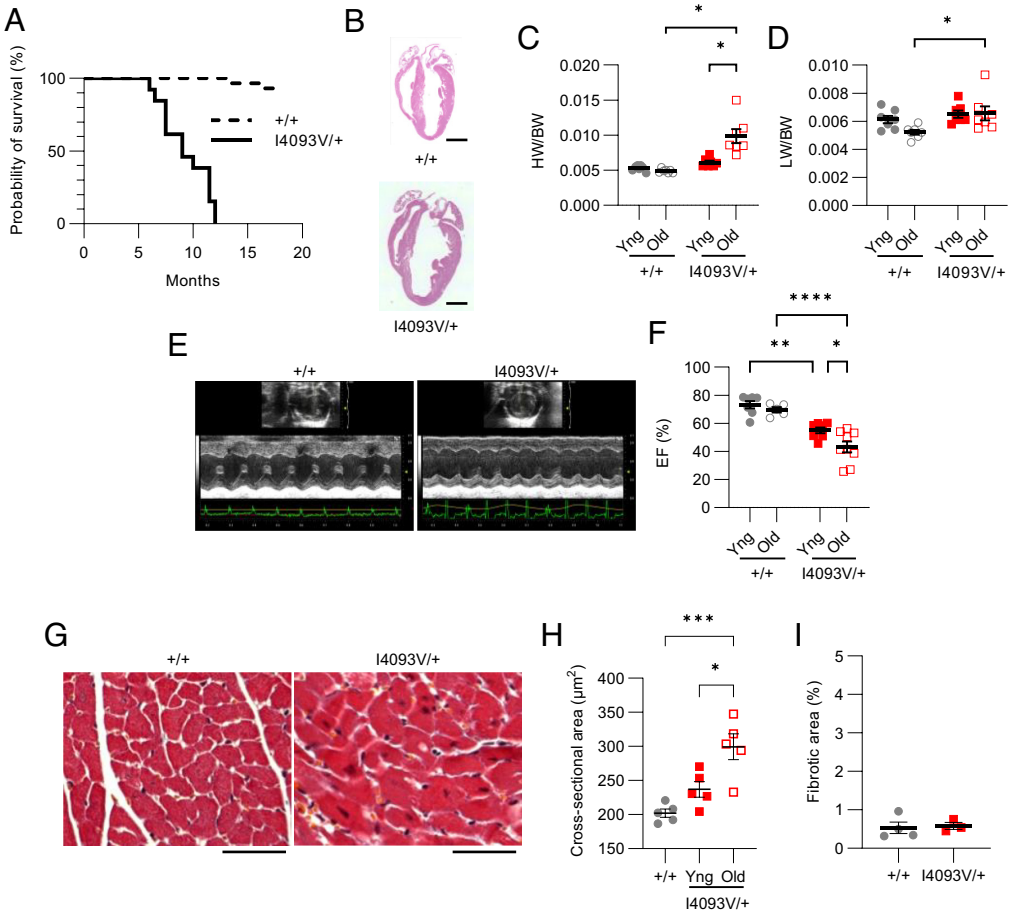

Fig. 3. *Ryr2*$^{I4093V/+}$ mice show significantly high mortality and age-related increase in heart weight and cellular dimension and decrease in left ventricular systolic function. (*A*) Kaplan–Meier survival curve for *Ryr2*$^{+/+}$ (n = 29) and *Ryr2*$^{I4093V/+}$ (n = 13) mice ($P < 0.0001$ by the log-rank test). (*B*) Representative heart histology of *Ryr2*$^{+/+}$ and *Ryr2*$^{I4093V/+}$ mice. (Scale bar denotes 2 mm.) (*C* and *D*) Heart weight (HW)/body weight (BW) (*B*) and lung weight (LW)/BW (*C*) in young (Yng: 2 to 3 mo old) and old (Old: 5 to 7 mo old) mice (n = 7 in each group). *$P < 0.05$ by Welch's ANOVA with Dunnett's T3 post hoc test for HW/BW, and one-way ANOVA with Tukey's post hoc test for LW/BW. (*E* and *F*) Echocardiographic measurements in young (n = 7) and old (n = 5) *Ryr2*$^{+/+}$ mice and young (n = 7) and old (n = 9) *Ryr2*$^{I4093V/+}$ mice. (*E*) Representative M-mode echocardiograms recorded at the tip of the papillary muscles. The graph shows the result of ejection fraction (EF) (*F*). *$P < 0.05$, **$P < 0.01$, and ****$P < 0.0001$ by one-way ANOVA with Tukey's post hoc test. (*G*) Representative images of Masson's trichrome–stained axial sections of *Ryr2*$^{+/+}$ and *Ryr2*$^{I4093V/+}$ left ventricles. (Scale bar denotes 50 μm.) (*H*) Quantification of the cardiomyocyte cross-sectional area from *Ryr2*$^{+/+}$, young (Yng: 2 to 3 mo old) *Ryr2*$^{I4093V/+}$, and old (Old: 5 to 7 mo old) *Ryr2*$^{I4093V/+}$ left ventricles (n = 5 in each group). *$P < 0.05$ and ***$P < 0.001$ by one-way ANOVA with Tukey's post hoc test. (*I*) Ratio of fibrotic area to global ventricular area in old *Ryr2*$^{+/+}$ (n = 4) and *Ryr2*$^{I4093V/+}$ (n = 3) mice. Means were compared by the *t*-test.

wild-type littermates to investigate how the I4093V mutation affects the channel activity of RyR2 at the subcellular level. To investigate the systolic Ca^{2+} properties of the single cardiomyocytes, Ca^{2+} transients under electrical stimulation at 0.33 Hz were analyzed by confocal microscopy. We observed the altered Ca^{2+} transient waveforms in *Ryr2*$^{I4093V/+}$ cardiomyocytes: The F/F_0 was slightly lower and the time to peak (TtP) and half decay time (DT_{50}) were significantly prolonged compared with those in *Ryr2*$^{+/+}$ cells (Fig. 4 *A–D* and *SI Appendix*, Fig. S7*A*). These findings were present to the same extent at both young and old ages (2 and 5 mo).

To determine the properties of diastolic Ca^{2+} leak, intracellular Ca^{2+} recordings were performed after field pacing at 3 Hz to apply the full SR Ca^{2+} load. We observed the well-organized, cell-wide Ca^{2+} waves with increasing frequency over time in the wild-type cardiomyocytes (Fig. 4 *E* and *F*). In contrast, *Ryr2*$^{I4093V/+}$ cardiomyocytes exhibited unstructured local Ca^{2+} increases that did not emerge in the form of cell-wide waves in the early diastolic phase (Fig. 4 *E* and *G*). Remarkably, we also found unstructured local Ca^{2+} increases with localized Ca^{2+} waves and Ca^{2+} sparks (*SI Appendix*, Fig. S7*B*) and ectopic Ca^{2+} activities, including early afterdepolarization (EAD) like Ca^{2+} signals (*SI Appendix*, Fig. S7*C*), in the decay phase of transients during field stimulation. For further elucidation of abnormal Ca^{2+} leak, spontaneous Ca^{2+} sparks with or without isoproterenol (ISO) were analyzed in quiescent cardiomyocytes. Spark frequency was significantly increased in *Ryr2*$^{I4093V/+}$ cardiomyocytes compared with that in *Ryr2*$^{+/+}$ cardiomyocytes under ISO exposure (*SI Appendix*, Fig. S8 *A* and *B*). Meanwhile, we found no significant differences in the spark mass, observable Ca^{2+} flux during one spark, between the two groups both without and with ISO treatment (*SI Appendix*, Fig. S8 *A* and *C*). We further measured SR Ca^{2+} leak and load by the Shannon's protocol (20) to determine the magnitude of total SR-$[Ca^{2+}]$-dependent Ca^{2+} leak via RyR2, including the part not observed as sparks. Diastolic Ca^{2+} leak from SR and SR Ca^{2+} load were significantly increased and decreased, respectively, in the mutant cardiomyocytes compared with those in wild-type cardiomyocytes, reflecting the enhancement of Ca^{2+} leak through the mutant RyR2 channels even in the context of reduced SR Ca^{2+} load throughout the postpacing diastolic phase (*SI Appendix*, Fig. S9 *A–D*).

For direct assessment of the Ca^{2+} sensitivity of heterotetrameric RyR2 in situ, we also performed recordings of spontaneous Ca^{2+} release events in permeabilized cardiomyocytes at the same intracellular Ca^{2+} concentration. In *Ryr2*$^{I4093V/+}$ cardiomyocytes, the number of Ca^{2+} release events was increased and the individual events were smaller than those in *Ryr2*$^{+/+}$ cardiomyocytes (*SI Appendix*, Fig. S10 *A–C*), probably as a result of enhanced cytosolic Ca^{2+} sensitivity in RyR2 mixmers.

Substantial Links between Ca^{2+} Dysregulation and APs in *Ryr2*$^{I4093V/+}$ Cardiomyocytes. To ascertain the direct relationship between abnormal subcellular Ca^{2+} kinetics and electrophysiological defects in the mutant cells, we proceeded to perform simultaneous recordings of APs and their evoked Ca^{2+} transients in single cardiomyocytes paced at 1 Hz under current-clamp mode. *Ryr2*$^{+/+}$ cardiomyocytes exhibited normal AP and Ca^{2+}-transient waveforms (Fig. 5*A*). In contrast, *Ryr2*$^{I4093V/+}$ cardiomyocytes exhibited cytosolic Ca^{2+} ($[Ca^{2+}]_{cyt}$) elevation in the decay phase between transients accompanied by abnormal $[Ca^{2+}]_{cyt}$ oscillations. This $[Ca^{2+}]_{cyt}$ irregularity was concurrent with prolonged depolarized potentials followed by triggered activities (Fig. 5*B*). Aging aggravated the occurrence of aberrant Ca^{2+} leak and simultaneous afterdepolarizations in the *Ryr2*$^{I4093V/+}$ cells (Fig. 5*C*). The incidence of the events, including early and/or delayed afterdepolarization and/or triggered activities, was significantly higher in both young and old *Ryr2*$^{I4093V/+}$ cardiomyocytes than in *Ryr2*$^{+/+}$ cardiomyocytes (Fig. 5 *D* and *E*). Individual AP duration (APD) was longer in the *Ryr2*$^{I4093V/+}$ cells than in the *Ryr2*$^{+/+}$ cells, and also similarly affected by age (Fig. 5 *F* and *G*). Detailed AP profiles are presented in *SI Appendix*, Fig. S11.

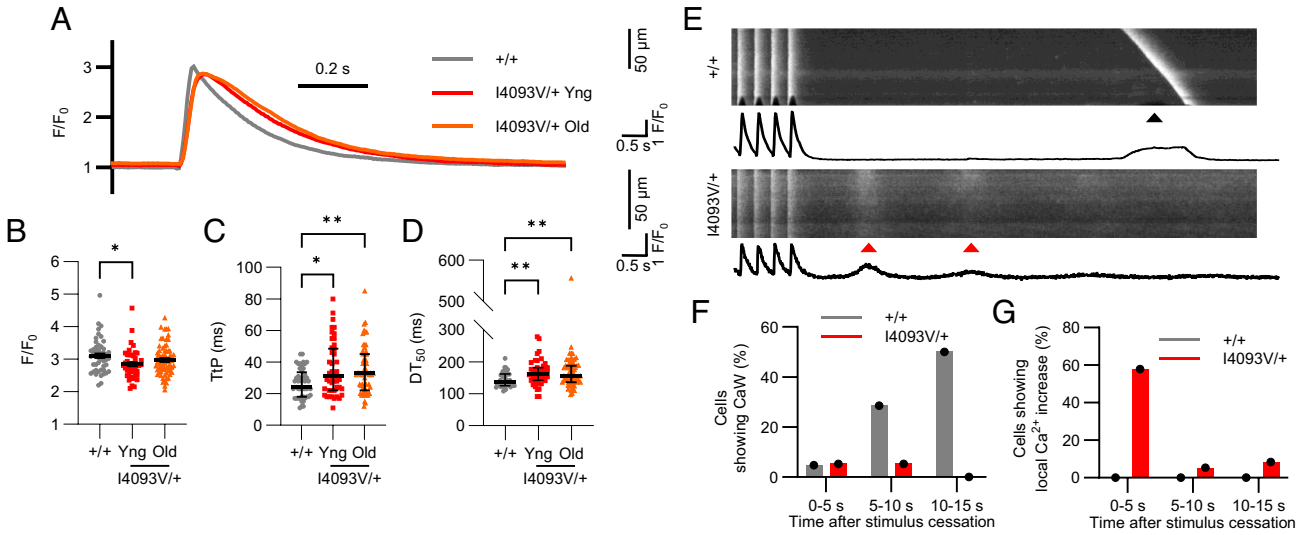

Fig. 4. Ca^{2+} handling characteristics in *Ryr2*$^{I4093V/+}$ cardiomyocytes. (*A*) Exemplar traces of Ca^{2+} transients under 0.33-Hz pacing in *Ryr2*$^{+/+}$, young (Yng: 2 to 3 mo old) *Ryr2*$^{I4093V/+}$, and old (Old: 5 to 7 mo old) *Ryr2*$^{I4093V/+}$ cardiomyocytes. (*B–D*) Parameters of Ca^{2+} transient properties of *Ryr2*$^{+/+}$ (n = 49), young *Ryr2*$^{I4093V/+}$ (n = 45), and old (n = 71) *Ryr2*$^{I4093V/+}$ cardiomyocytes (3 mice in each group). *P < 0.05 by one-way ANOVA with Tukey's post hoc test for F/F_0. *P < 0.05 and **P < 0.01 by the Kruskal–Wallis test with Dunn's post hoc test for time to peak (TtP) and half decay time (DT_{50}). (*E*) Representative line scan images of spontaneous Ca^{2+} activities in *Ryr2*$^{+/+}$ and *Ryr2*$^{I4093V/+}$ cardiomyocytes during postpacing period after 3-Hz field stimulation. The black arrowhead indicates cell-wide Ca^{2+} wave. The red arrowheads indicate local Ca^{2+} increase. (*F*) Fraction of cells showing spontaneous Ca^{2+} wave (CaW) during the postpacing period in *Ryr2*$^{+/+}$ (n = 21) and *Ryr2*$^{I4093V/+}$ (n = 19) cardiomyocytes (four mice in each group). Data are shown every 5 s after stimulus cessation. Black dots indicate actual values (%). (*G*) Fraction of cells showing local Ca^{2+} increase during the postpacing period in *Ryr2*$^{+/+}$ (n = 21) and *Ryr2*$^{I4093V/+}$ (n = 19) cardiomyocytes (four mice in each group). Data are shown every 5 s after stimulus cessation. Black dots indicate actual values (%).

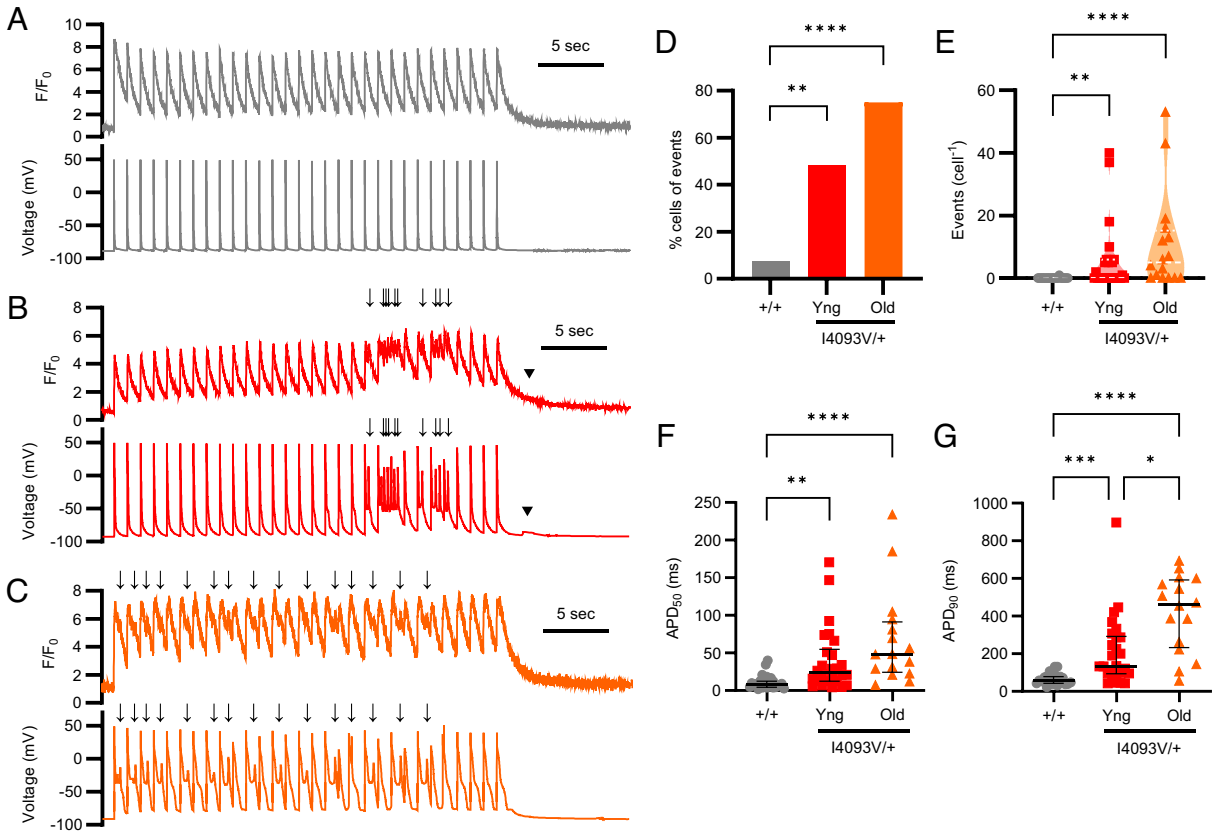

Fig. 5. Simultaneous recordings of APs and their evoked Ca^{2+} transients in isolated cardiomyocytes. (*A–C*) Representative recordings of Ca^{2+} transients and APs of *Ryr2*$^{+/+}$ (*A*), young (Yng: 2 to 3 mo old) *Ryr2*$^{I4093V/+}$ (*B*), and old (Old: 5 to 7 mo old) *Ryr2*$^{I4093V/+}$ cardiomyocytes (*C*). Arrows indicate EAD or triggered activities and their associated Ca^{2+} oscillations. Arrowheads indicate delayed afterdepolarization. (*D*) Percentage of cells with events, including early and/or delayed afterdepolarization and/or triggered activities in *Ryr2*$^{+/+}$ (n = 26), young *Ryr2*$^{I4093V/+}$ (n = 27), and old *Ryr2*$^{I4093V/+}$ (n = 16) groups (three mice in each group). $^{**}P < 0.01$ and $^{****}P < 0.0001$ by Fisher's exact test. (*E*) Event frequency of *Ryr2*$^{+/+}$ (n = 26), young *Ryr2*$^{I4093V/+}$ (n = 27), and old *Ryr2*$^{I4093V/+}$ (n = 16) cardiomyocytes (three mice in each group). $^{**}P < 0.01$ and $^{****}P < 0.0001$ by the Kruskal–Wallis test with Dunn's post hoc test. (*F* and *G*) AP durations at 50% and 90% repolarization (APD_{50} and APD_{90}) in *Ryr2*$^{+/+}$ (n = 26), young *Ryr2*$^{I4093V/+}$ (n = 26), and old *Ryr2*$^{I4093V/+}$ (n = 16) cardiomyocytes (three mice in each group). $^{*}P < 0.05$, $^{**}P < 0.01$, $^{***}P < 0.001$, and $^{****}P < 0.0001$ by the Kruskal–Wallis test with Dunn's post hoc test.

Taking these findings together, the aberrant Ca^{2+} fluctuations during both systole and diastole in *Ryr2*$^{I4093V/+}$ cardiomyocytes were likely to be a crucial driving factor in the susceptibility of the mutant mice to arrhythmia. Moreover, aging-aggravated APD prolongation elevated the level of aberrant electrical substrate in the mutant cardiomyocytes.

Frequent Ca^{2+} Oscillations with Decreased $[Ca^{2+}]_{ER}$ in HEK293 Cells Expressing I4093V *Ryr2*. To gain insight into the molecular basis behind the detrimental arrhythmias in *Ryr2*$^{I4093V/+}$ mice, wild-type and mutant *Ryr2* (c.12277A>G, p.I4093V) were inducibly expressed in HEK293 cells, and $[Ca^{2+}]_{cyt}$ and ER Ca^{2+} ($[Ca^{2+}]_{ER}$) signals were measured using our routine method (21–23). After 24 h of induction, cells expressing wild-type RyR2 exhibited spontaneous $[Ca^{2+}]_{cyt}$ oscillations accompanied by a concomitant decrease in $[Ca^{2+}]_{ER}$ signal from the threshold to the nadir level (Fig. 6*A*), which indicated that Ca^{2+} was released from the ER via the RyR2 channels. Cells expressing I4093V RyR2 manifested more frequent and smaller Ca^{2+} oscillations and lower $[Ca^{2+}]_{ER}$ levels than the wild-type RyR2 cells (Fig. 6 *A* and *B*). Massive Ca^{2+} release from the ER was induced by caffeine treatment in the wild-type RyR2 cells, whereas the I4093V RyR2 cells exhibited a diminished response to caffeine as a reflection of the markedly lower $[Ca^{2+}]_{ER}$ (Fig. 6*A*). The threshold and nadir of $[Ca^{2+}]_{ER}$ were significantly decreased in the I4093V RyR2 cells compared with those in the wild-type RyR2 cells (Fig. 6*C*). The greater decrease in $[Ca^{2+}]_{ER}$ in the I4093V RyR2 cells compared to the wild-type was confirmed even at shorter induction times (*SI Appendix*, Fig. S12), which indicates that ER Ca^{2+} release from I4093V RyR2 severely reduces $[Ca]_{ER}$ in an expression-dependent manner. These I4093V RyR2 characteristics have been suggested to represent the strong gain-of-function phenotype of CPVT mutants (23, 24).

Channel Dysfunction of I4093V RyR2. We subsequently measured the amount of Ca^{2+}-dependent [^{3}H]ryanodine binding to microsomes derived from RyR2-transfected HEK293 cells. Because ryanodine specifically binds to the open channel, [^{3}H]ryanodine binding is used to quantitatively evaluate the activity of RyR2 channels (22, 25). I4093V RyR2 showed biphasic Ca^{2+} dependence with enhanced Ca^{2+} sensitivity to activation compared with wild-type RyR2 (Fig. 6*D*). In particular, the increase in Ca^{2+} sensitivity caused by the I4093V mutation was quite large compared with previously reported CPVT-linked mutations (23). In addition, the three parameters for CICR activity were significantly changed in the mutant RyR2 (*SI Appendix*, Fig. S13). The estimated CICR activity of the mutant RyR2 using these parameters and Equation 1 (see the *Materials and Methods* in *SI Appendix*) was significantly greater than that of wild-type RyR2 at resting Ca^{2+} (pCa 7), supporting the profoundly high Ca^{2+} sensitivity of I4093V RyR2 (23) (Fig. 6*E*). These results suggest that the markedly enhanced sensitivity to cytosolic Ca^{2+} plays a vital role in the substantial arrhythmogenic potential of the I4093V mutation.

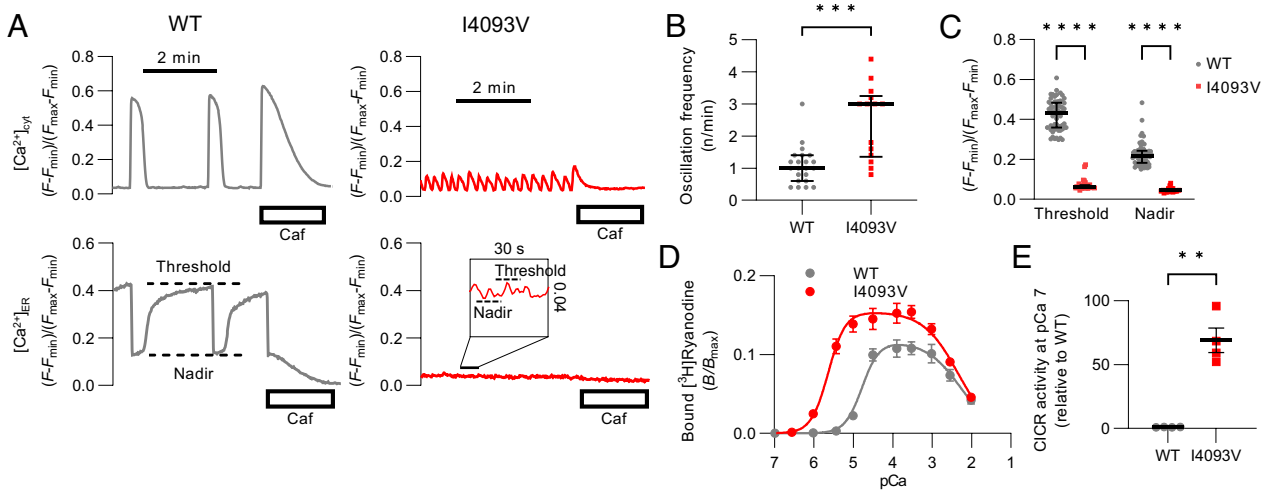

Fig. 6. I4093V RyR2-expressing HEK293 cells and RyR2-I4093V channels. (*A*) Representative $[Ca^{2+}]_{cyt}$ and $[Ca^{2+}]_{ER}$ signals from G-GECO1.1 and R-CEPIA1er, respectively, in wild-type (WT) RyR2-expressing (*Left*) or I4093V RyR2-expressing (*Right*) HEK293 cells. Ca^{2+} signals in individual cells are expressed as $(F–F_{min})/(F_{max}–F_{min})$, where F_{min} and F_{max} were obtained at the end of measurements. *Top* and *Bottom* graphs show the $[Ca^{2+}]_{cyt}$ and $[Ca^{2+}]_{ER}$ signals in normal Krebs solution followed by caffeine-containing Krebs solution, respectively. The box bar indicates treatment with caffeine (10 mM). Upper and lower limits of $[Ca^{2+}]_{ER}$ under baseline conditions are indicated as Threshold and Nadir with dotted lines (in the magnified graph for I4093V cells), respectively. (*B*) Oscillation frequency in the WT (n = 22) and I4093V (n = 14) RyR2 cells. ***$P < 0.001$ by the Mann–Whitney U test. (*C*) Threshold and Nadir (n = 65 and 36 for WT and I4093V cells, respectively) of $[Ca^{2+}]_{ER}$ under baseline conditions. ****$P < 0.0001$ by the Mann–Whitney U test for Threshold and Nadir. (*D*) Ca^{2+}-dependent [^{3}H]ryanodine binding. The line graph shows data from WT RyR2- or I4093V RyR2-expressing HEK293 cells (n = 4 in each group). Data are given as mean ± SD. (*E*) CICR activity for WT RyR2 and I4093V RyR2 at pCa 7 (resting). Individual values were calculated using Equation **1** with the obtained CICR parameters (see the Materials and Methods in *SI Appendix*). The RyR2-I4093V channel shows approximately 60-fold higher activity than the WT channel. **$P < 0.01$ by the *t*-test with Welch's correction.

We also confirmed the expression level and degree of post-translational modification of intracellular Ca^{2+}-regulatory molecules in *Ryr2*$^{I4093V/+}$ cardiomyocytes. There was no significant difference between the wild-type and mutant groups (*SI Appendix*, Fig. S14), which suggests that the most dominant contributor to the disruption of Ca^{2+} regulatory mechanisms in *Ryr2*$^{I4093V/+}$ cardiomyocytes is the aberrant function of I4093V RyR2 channels.

Drug Efficacy Assessment using *Ryr2*$^{I4093V/+}$ Mice. We examined the applicability of *Ryr2*$^{I4093V/+}$ mice in evaluating antiarrhythmic drug efficacy. A drug already proven to be effective for CPVT, flecainide (26), and the direct RyR-targeting drug, dantrolene (27), were selected for this experiment. Because our model exhibited spontaneous VAs, we employed a simple protocol in which ECG recordings of the anesthetized *Ryr2*$^{I4093V/+}$ mice at 5 to 6 mo of age were performed for 5 min immediately before (Pre) and after (Post) intraperitoneal injection of each drug. Fig. 7*A* shows representative ECG and HR results obtained from each test period. VAs were observed as the coincidence of ECG amplitude change and HR deviation. The frequencies of VAs were significantly reduced by treatment with flecainide (Fig. 7*B*) or dantrolene (Fig. 7*C*). These test results suggest that the present model can be utilized for the evaluation of drug efficacy.

Discussion

In the present study, an ECG-based screen of a randomly mutagenized mouse library identified one pedigree that exhibited spontaneous BVT and a poor prognosis of less than 1 y. Our mouse model harbors a mutation of *Ryr2*, which showed a high incidence of VT without electrical or pharmacological stimulation, followed by spontaneous SCD. Genetic analysis successfully revealed a missense mutation in *Ryr2* (c.12277A>G, p.I4093V) as the causative factor. Vulnerability to VA in *Ryr2*$^{I4093V/+}$ mice was exacerbated with age. Furthermore, the mutant pedigree had age-related cardiac enlargement and decreased cardiac contractions with myocyte hypertrophy. *Ryr2*$^{I4093V/+}$ cardiomyocytes showed excessive Ca^{2+} leakage at the systolic and diastolic phases observed as postpacing Ca^{2+} leak and Ca^{2+}-transient waveform changes. This defect of Ca^{2+} homeostasis was confirmed to directly induce triggered activities as a source of arrhythmia. The channel-opening activity of I4093V RyR2 showed prominently higher cytosolic Ca^{2+} sensitivity than wild-type RyR2. As a result of abnormal Ca^{2+} leakage through the mutant channel, small, frequent Ca^{2+} oscillations were observed and ER Ca^{2+} loads were diminished in the I4093V RyR2-expressing HEK293 cells. *Ryr2*-I4093V was found to be a gain-of-function mutation that could be the main cause of the detrimental VA. In addition, we demonstrated the applicability of the present model for evaluating the efficacy of drugs in vivo to prevent VAs in IASs.

A forward-genetics study using a large-scale mutagenized vertebrate cohort has been conducted to unveil the genes causative of various cardiac phenotypes (28, 29). We previously performed an electroencephalogram/electromyogram-based screen of an ENU-mutagenized mouse library and identified the sleep-regulating genes *SIK3* and *NALCN* (13). Our arrhythmia pedigree was established from the same library using a forward-genetics strategy. Although only one pedigree showed evidence of heritability of the VT, genetic analysis comprising linkage analysis and whole-exome sequencing accurately revealed the causative mutation. Several mutations causative of IASs have been reported to date, and the *Ryr2* mutations account for 65% of the genetic causes of CPVT (4). However, the present *Ryr2* mutation has not been reported as a cause of cardiac phenotypes. The corresponding missense mutation I4094V in human *RYR2* was reported to be a cancer-promoting mutation in a cohort study, as cataloged in the COSMIC database (30). Another study described I4138T, the homologous mutation in human *RYR1*, as causing malignant hyperthermia (31), which is a skeletal muscle disorder that primarily results from gain-of-function *RYR1* mutations. The phenotype of the *Ryr2*$^{I4093V/+}$ pedigree remained the same after more than 20 generations of backcrossing with wild-type C57BL/6N mice, which rules out the possible involvement of ENU-induced variations in other genetic loci. Altogether,

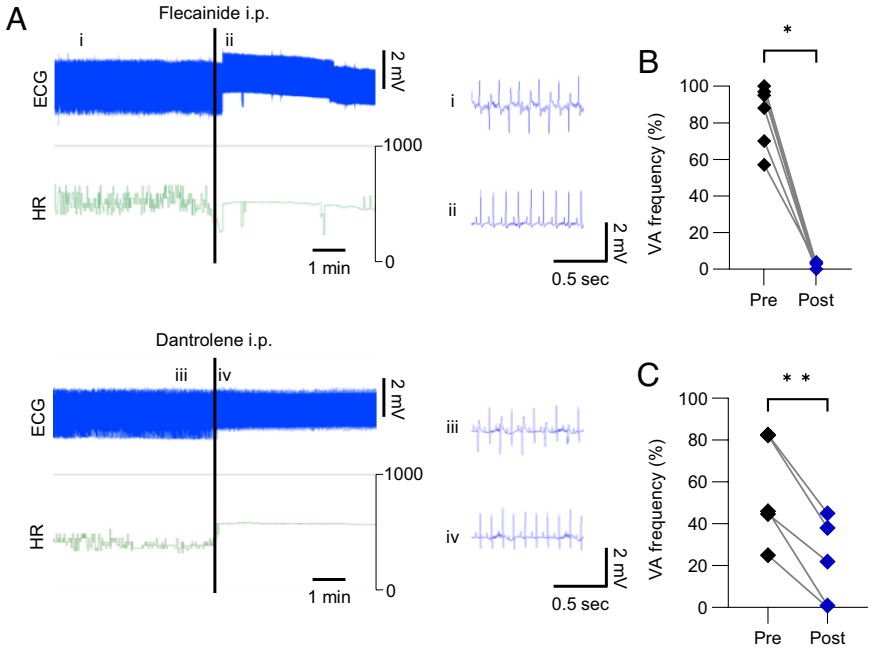

Fig. 7. Utilization of *Ryr2*$^{I4093V/+}$ mice for drug efficacy assessment. (*A*) Representative ECG traces with HR changes in each drug test period. Time-expanded ECGs show BVT (i), sinus rhythm (ii and iv), and PVC bigeminy (iii). (*B* and *C*) VA frequency for 5 min before (Pre) and after (Post) intraperitoneal injection (i.p.) of flecainide (*B*) (n = 6) or dantrolene (*C*) (n = 5). *$P < 0.05$ by the Wilcoxon matched-pairs signed-rank test for flecainide treatment and **$P < 0.01$ by the paired *t*-test for dantrolene treatment.

we conclude that *Ryr2*-I4093V mutation is the malign genetic defect behind the life-threatening arrhythmias.

The IAS mouse model showed age-related susceptibility to VAs: Young mice (2 mo old) exhibited arrhythmia under adrenergic stress, resembling CPVT, while older mice developed frequent, spontaneous VAs. This age-related vulnerability to arrhythmia in *Ryr2*$^{I4093V/+}$ mice possibly exacerbated the ventricular hypertrophy, which might explain the QRS and T morphological changes with age (32, 33). At the cellular level, *Ryr2*$^{I4093V/+}$ cardiomyocytes showed APD prolongation without changes in AP amplitude or dV/dt max (Fig. 5 *F* and *G* and *SI Appendix*, Fig. S11), suggesting that this repolarization abnormality was additionally responsible for QTc prolongation. The cell size of the *Ryr2*$^{I4093V/+}$ cardiomyocytes was enlarged, supported by the increased capacitance (*SI Appendix*, Fig. S11) and dimensional increment (Fig. 3 *G* and *H*). This is considered to be a cause of the cardiomegaly. We also found impairment of LV contraction with age and high cardiac mortality in the *Ryr2*$^{I4093V/+}$ mice. Numerous studies aimed at analyzing arrhythmias have described the use of mouse models, including several models harboring *Ryr2* mutations (34). With most established models, some form of stimulation is required for the induction of VT in in vivo experiments (35–37). Conversely, although age-related cardiac remodeling may be a contributing factor, BVT was spontaneously observed with a high frequency in *Ryr2*$^{I4093V/+}$ mice. Therefore, this mouse model appears to be one of the most ventricular-arrhythmia-prone mice. Certain human *RYR2* mutations have been described as causing arrhythmogenic right ventricular cardiomyopathy or dilated cardiomyopathy in previous reports (38, 39), although no mouse models with *Ryr2* mutations have been reported to have a reduced LVEF. We postulated that the model's tissue level and cellular remodeling in the heart might be rooted in the tremendously high frequency of VAs mediated by abnormal Ca^{2+} homeostasis, similar to the pathology of arrhythmia-induced cardiomyopathy (40). This defect might lead to cardiac overload and consequential pulmonary edema, which would exacerbate the arrhythmogenicity. Although a further confirmation study is required, the *Ryr2*$^{I4093V/+}$ mouse pedigree appears to be an excellent model of a critically severe form of IASs.

The likely explanation for the severe arrhythmogenicity of the I4093V mutation is that the RyR2 activity of I4093V is greatly enhanced. From the result of [^{3}H]ryanodine binding assay, we observed a great shift of the binding activity of the mutant RyR2 in the direction of the channel opening dependent on cytosolic Ca^{2+} sensitivity compared with that of the wild-type RyR2 (Fig. 6*D*). The profound increase in Ca^{2+} sensitivity at physiological Ca^{2+} concentration is evidence for the I4093V mutation as a strong gain-of-function. We have previously reported that mutant RyR2 activities at resting Ca^{2+} concentration (A_{rest}), determined by the [^{3}H]ryanodine binding assay, correlate well with arrhythmia severity in patients (23). The A_{rest} of the I4093V mutation is about 60 times higher than that of the wild type and is predicted to be extremely severe, suggesting that the present mutation is highly pathogenic. Correspondingly, HEK293 cells expressing I4093V RyR2 show severe ER Ca^{2+} depletion 24 h after induction. In addition, permeabilized cardiomyocytes also show small and frequent fast Ca^{2+} waves and are also prone to Ca^{2+} leak, supporting the high channel activity of mixmers of wild-type and I4093V RyR2 in myocardial cells. In terms of the molecular structural aspects of RyR2, I4093 is located in a helix of the central domain, which is alongside the helices where the residues comprising the Ca^{2+} binding pocket, E3847 and E3921, reside (*SI Appendix*, Fig. S2) (41). Since I4093V RyR2 exhibited an increased Ca^{2+} sensitivity for activation (Fig. 6*D*), the mutation might shift the positions of the helices to increase the Ca^{2+} binding affinity for the channel opening.

In the Ca^{2+} signaling analysis, cardiomyocytes from typical CPVT model mice with RyR2 mutations are known to show increased frequencies of Ca^{2+} waves and Ca^{2+} sparks during the diastolic phase of Ca^{2+} transients, which causes delayed afterdepolarization (19). Surprisingly, in the I4093V cardiomyocytes, no clear Ca^{2+} wave was observed, but EAD and EAD-triggered

activity were frequently observed during the repolarizing phase of the APs. However, closer examination revealed characteristic Ca^{2+} abnormalities, i.e., amorphous local Ca^{2+} increases and incomplete small Ca^{2+} waves, were frequently observed after high-frequency stimulation. This observation is very similar to the abnormal Ca^{2+} signals reported in cardiomyocytes from homozygous R33Q-calsequestrin 2 knock-in mice, one of the severely pathogenic models of CPVT (42). A study has reported that EAD can be generated by the Na^{+}/Ca^{2+} exchanger (NCX) in situations where spontaneous SR Ca^{2+} release tends to develop before repolarization is complete (43, 44). Taking these findings together, it would be considered that *Ryr2*$^{I4093V/+}$ cardiomyocytes generate EADs induced by forward-mode NCX due to excessive SR Ca^{2+} release from profoundly activated I4093V RyR2, even during the systolic period.

Heart failure is associated with electrical remodeling causing APD prolongation (45), and thus the cardiac overload that the *Ryr2*$^{I4093V/+}$ mice exhibited would accelerate the generation of EADs. We also consider that prolonged APD partially contributes to the delayed Ca^{2+} transient decay. However, young *Ryr2*$^{I4093V/+}$ cardiomyocytes already exhibited a prolonged decay time of Ca^{2+} transients equivalent to that in old *Ryr2*$^{I4093V/+}$ cardiomyocytes (Fig. 4*D*). In addition, the prolongation of APD was worse in the old mutant cells than in the young ones (Fig. 5 *F* and *G*), which indicated that Ca^{2+}-kinetic abnormality may precede AP aberrancy. Because the expression levels of Ca^{2+} regulatory proteins did not differ significantly between *Ryr2*$^{+/+}$ and *Ryr2*$^{I4093V/+}$ ventricles, the *Ryr2*-I4093V mutation is likely to be the main cause of the Ca^{2+} dysregulation underlying arrhythmogenesis. Overall, these findings suggest that *Ryr2*$^{I4093V/+}$ mice have aberrant Ca^{2+} homeostasis and electrical properties at the subcellular level.

SCD remains an important public health problem worldwide, and previously described genetic autopsies of victims of SCD have identified *RYR2* as a major candidate gene in young people (46, 47). Genetic defects in *RYR2* have been reported to be the major cause of CPVT (16) and one of the causes of arrhythmogenic right ventricular cardiomyopathy (38). Hence, the *Ryr2*$^{I4093V/+}$ mouse should be advantageous in research into SCD, IASs, and even arrhythmia-induced cardiomyopathy. On this basis, we tested whether the present model could be applied in drug efficacy assessments. A major antiarrhythmic drug for CPVT, flecainide, successfully reduced VA burden in our test protocol. Dantrolene, which has more direct effects on RyR, also suppressed arrhythmogenicity in our model mice. The clinical applicability of this mouse model is partially limited by the absence of the corresponding RyR2 variant in humans and by some features of baseline ECG abnormalities, ventricular systolic dysfunction, and age-related aggravation of cardiac defects, which are different from those of the typical CPVT. Nevertheless, the results of the drug tests suggest that *Ryr2*$^{I4093V/+}$ mice are a practical option for assessing the efficacy of therapies for SCD from severe IASs.

In conclusion, using a forward-genetics strategy, we successfully established a mouse model of IASs that exhibits spontaneous BVT and SCD within 1 y after birth. Analysis suggested that the primary pathogenesis is caused by excessive Ca^{2+} leak due to the novel missense mutation in *Ryr2*. We believe that the *Ryr2*$^{I4093V/+}$ mice may prove useful for research into arrhythmogenic mechanisms and the development of new therapies for IASs with an emphasis on unveiling drug mechanisms and the preclinical testing of drugs.

Materials and Methods

The detailed methods are available in *SI Appendix*. All supporting data from this study are available from the corresponding author upon reasonable request.

The animal study was approved by the Institutional Animal Care and Use Committee of the University of Tsukuba. A randomly mutagenized mouse library was established by in vitro fertilization with the sperm of C57BL/6J (B6J) mice treated with ENU and eggs from C57BL/6N (B6N) mice. The obtained F_1 offspring were screened by ECG for an arrhythmia phenotype. N_2 offspring from the F_1 arrhythmia mice were examined by linkage analysis and whole-exome sequencing to identify a gene causative of the arrhythmia. The detailed methods of mouse genotyping and phenotyping, Ca^{2+} imaging, patch-clamp recording, ryanodine binding analysis, and drug efficacy assessment are described in Supplementary Information. Statistical analysis was performed in SPSS version 26 (IBM Co. Ltd.) or Prism 9 (GraphPad Software), and the tests used are indicated in each figure legend.

Please see the Expanded Methods in *SI Appendix*.

Data, Materials, and Software Availability. All study data are included in the article and/or *SI Appendix*.

ACKNOWLEDGMENTS. We are grateful to Mrs. Yumi Isaka and Mrs. Akiko Miyamoto for their technical assistance. We thank the University of Tsukuba Laboratory Animal Resource Center for their assistance in maintaining mouse colonies. This work was supported by the World Premier International Research Center Initiativefrom Ministry of Education, Culture, Sports, Science and Technology to M.Y.; Japan Agency for Medical Research and Development (JP21zf0127005 to M.Y.); Japan Society for the Promotion of Science (JSPS) Grants-in-Aid for Scientific Research (17H06095 and 22H04918 to M.Y. and H.F., 16H05045 to K.A., 19H03404 to T.M., 19K07105 to N.K., and 23659410 to N.M.); Basis for Supporting Innovative Drug Discovery and Life Science Research (JP21am0101080 to T.M.); the Vehicle Racing Commemorative Foundation (6237 to T.M.); and Funding Program for World-Leading Innovative R&D on Science and Technology from JSPS to M.Y.

Author affiliations: [a]Department of Cardiology, Faculty of Medicine, University of Tsukuba, Tsukuba 305-8575, Japan; [b]Department of Cellular and Molecular Pharmacology, Juntendo University Graduate School of Medicine, Tokyo 113-8421, Japan; [c]Department of Physiology, Tokyo Medical University, Tokyo 160-8402, Japan; [d]International Institute for Integrative Sleep Medicine, University of Tsukuba, Tsukuba 305-8575, Japan; [e]Technology and Development Team for Mouse Phenotype Analysis, RIKEN BioResource Center, Tsukuba 305-0074, Japan; [f]Department of Animal Experimentation, Foundation for Biomedical Research and Innovation at Kobe, Kobe 650-0047, Japan; and [g]Department of Cardiology, Keio University School of Medicine, Tokyo 160-8582, Japan

1. S. G. Priori *et al.*, 2015 ESC Guidelines for the management of patients with ventricular arrhythmias and the prevention of sudden cardiac death: The Task Force for the Management of Patients with Ventricular Arrhythmias and the Prevention of Sudden Cardiac Death of the European Society of Cardiology (ESC). Endorsed by: Association for European Paediatric and Congenital Cardiology (AEPC). *Eur. Heart J.* **36**, 2793–2867 (2015).
2. M. K. Stiles *et al.*, 2020 APHRS/HRS expert consensus statement on the investigation of decedents with sudden unexplained death and patients with sudden cardiac arrest, and of their families. *Heart Rhythm* **18**, e1–e50 (2021).
3. P. J. Schwartz *et al.*, Inherited cardiac arrhythmias. *Nat. Rev. Dis. Primers* **6**, 58 (2020).
4. M. J. Ackerman *et al.*, HRS/EHRA expert consensus statement on the state of genetic testing for the channelopathies and cardiomyopathies this document was developed as a partnership between the Heart Rhythm Society (HRS) and the European Heart Rhythm Association (EHRA). *Heart Rhythm* **8**, 1308–1339 (2011).
5. C. R. Bezzina *et al.*, Common variants at SCN5A-SCN10A and HEY2 are associated with Brugada syndrome, a rare disease with high risk of sudden cardiac death. *Nat. Genet.* **45**, 1044–1049 (2013).
6. B. Gray, E. R. Behr, New insights into the genetic basis of inherited arrhythmia syndromes. *Circ. Cardiovasc. Genet.* **9**, 569–577 (2016).
7. G. F. Tomaselli, Introduction to a compendium on sudden cardiac death: Epidemiology, mechanisms, and management. *Circ. Res.* **116**, 1883–1886 (2015).
8. S. M. Al-Khatib *et al.*, 2017 AHA/ACC/HRS guideline for management of patients with ventricular arrhythmias and the prevention of sudden cardiac death: executive summary: A report of the American College of Cardiology/American Heart Association Task Force on Clinical Practice Guidelines and the Heart Rhythm Society. *Circulation* **138**, e210–e271 (2018).
9. J. S. Takahashi, L. H. Pinto, M. H. Vitaterna, Forward and reverse genetic approaches to behavior in the mouse. *Science* **264**, 1724–1733 (1994).
10. D. Y. Stainier, Zebrafish genetics and vertebrate heart formation. *Nat. Rev. Genet.* **2**, 39–48 (2001).
11. Y. Gondo, Trends in large-scale mouse mutagenesis: From genetics to functional genomics. *Nat. Rev. Genet.* **9**, 803–810 (2008).
12. J. S. Takahashi, K. Shimomura, V. Kumar, Searching for genes underlying behavior: Lessons from circadian rhythms. *Science* **322**, 909–912 (2008).

13. H. Funato *et al.*, Forward-genetics analysis of sleep in randomly mutagenized mice. *Nature* **539**, 378–383 (2016).
14. D. A. Eisner, J. L. Caldwell, K. Kistamás, A. W. Trafford, Calcium and excitation-contraction coupling in the heart. *Circ. Res.* **121**, 181–195 (2017).
15. W. Peng *et al.*, Structural basis for the gating mechanism of the type 2 ryanodine receptor RyR2. *Science* **354**, aah5324 (2016).
16. S. G. Priori *et al.*, Mutations in the cardiac ryanodine receptor gene (hRyR2) underlie catecholaminergic polymorphic ventricular tachycardia. *Circulation* **103**, 196–200 (2001).
17. D. Jiang, W. Chen, R. Wang, L. Zhang, S. R. Chen, Loss of luminal Ca^{2+} activation in the cardiac ryanodine receptor is associated with ventricular fibrillation and sudden death. *Proc. Natl. Acad. Sci. U.S.A.* **104**, 18309–18314 (2007).
18. N. Sumitomo *et al.*, Catecholaminergic polymorphic ventricular tachycardia: Electrocardiographic characteristics and optimal therapeutic strategies to prevent sudden death. *Heart* **89**, 66–70 (2003).
19. S. E. Lehnart *et al.*, Leaky Ca^{2+} release channel/ryanodine receptor 2 causes seizures and sudden cardiac death in mice. *J. Clin. Invest.* **118**, 2230–2245 (2008).
20. T. R. Shannon, K. S. Ginsburg, D. M. Bers, Quantitative assessment of the SR Ca^{2+} leak-load relationship *Circ. Res.* **91**, 594–600 (2002).
21. A. Uehara *et al.*, Extensive Ca^{2+} leak through K4750Q cardiac ryanodine receptors caused by cytosolic and luminal Ca^{2+} hypersensitivity. *J. Gen. Physiol.* **149**, 199–218 (2017).
22. Y. Nozaki *et al.*, Co-phenotype of left ventricular non-compaction cardiomyopathy and atypical catecholaminergic polymorphic ventricular tachycardia in association with R169Q, a Ryanodine receptor type 2 missense mutation. *Circ. J.* **84**, 226–234 (2020).
23. N. Kurebayashi *et al.*, Cytosolic Ca^{2+}-dependent Ca^{2+} release activity primarily determines the ER Ca^{2+} level in cells expressing the CPVT-linked mutant RYR2. *J. Gen. Physiol.* **154**, e202112869 (2022).
24. T. Murayama *et al.*, A tryptophan residue in the caffeine-binding site of the ryanodine receptor regulates Ca(2+) sensitivity. *Commun. Biol.* **1**, 98 (2018).
25. Y. Fujii *et al.*, A type 2 ryanodine receptor variant associated with reduced Ca(2+) release and short-coupled torsades de pointes ventricular arrhythmia. *Heart Rhythm* **14**, 98–107 (2017).
26. P. J. Kannankeril *et al.*, Efficacy of flecainide in the treatment of catecholaminergic polymorphic ventricular tachycardia: A randomized clinical trial. *JAMA Cardiol.* **2**, 759–766 (2017).
27. S. Kobayashi *et al.*, Dantrolene, a therapeutic agent for malignant hyperthermia, markedly improves the function of failing cardiomyocytes by stabilizing interdomain interactions within the ryanodine receptor. *J. Am. Coll. Cardiol.* **53**, 1993–2005 (2009).
28. Y. Li *et al.*, Global genetic analysis in mice unveils central role for cilia in congenital heart disease. *Nature* **521**, 520–524 (2015).
29. T. Dahme, H. A. Katus, W. Rottbauer, Fishing for the genetic basis of cardiovascular disease. *Dis. Model. Mech.* **2**, 18–22 (2009).
30. J. G. Tate *et al.*, COSMIC: The catalogue of somatic mutations in cancer. *Nucl. Acids Res.* **47**, D941–D947 (2019).
31. R. Robinson, D. Carpenter, M. A. Shaw, J. Halsall, P. Hopkins, Mutations in RYR1 in malignant hyperthermia and central core disease. *Hum. Mutat.* **27**, 977–989 (2006).
32. P. Sysa-Shah, L. L. Sørensen, M. R. Abraham, K. L. Gabrielson, Electrocardiographic characterization of cardiac hypertrophy in mice that overexpress the ErbB2 receptor tyrosine kinase. *Comp. Med.* **65**, 295–307 (2015).
33. R. F. Wiegerinck *et al.*, Larger cell size in rabbits with heart failure increases myocardial conduction velocity and QRS duration. *Circulation* **113**, 806–813 (2006).
34. A. Kushnir, M. J. Betzenhauser, A. R. Marks, Ryanodine receptor studies using genetically engineered mice. *FEBS Lett.* **584**, 1956–1965 (2010).
35. M. Cerrone *et al.*, Bidirectional ventricular tachycardia and fibrillation elicited in a knock-in mouse model carrier of a mutation in the cardiac ryanodine receptor. *Circ. Res.* **96**, e77–e82 (2005).
36. P. J. Kannankeril *et al.*, Mice with the R176Q cardiac ryanodine receptor mutation exhibit catecholamine-induced ventricular tachycardia and cardiomyopathy. *Proc. Natl. Acad. Sci. U.S.A.* **103**, 12179–12184 (2006).
37. S. Nishimura *et al.*, Mutation-linked, excessively tight interaction between the calmodulin binding domain and the C-terminal domain of the cardiac ryanodine receptor as a novel cause of catecholaminergic polymorphic ventricular tachycardia. *Heart Rhythm* **15**, 905–914 (2018).
38. N. Tiso *et al.*, Identification of mutations in the cardiac ryanodine receptor gene in families affected with arrhythmogenic right ventricular cardiomyopathy type 2 (ARVD2). *Hum. Mol. Genet.* **10**, 189–194 (2001).
39. Z. A. Bhuiyan *et al.*, Expanding spectrum of human RYR2-related disease: New electrocardiographic, structural, and genetic features. *Circulation* **116**, 1569–1576 (2007).
40. J. F. Huizar, K. A. Ellenbogen, A. Y. Tan, K. Kaszala, Arrhythmia-induced cardiomyopathy: JACC state-of-the-art review. *J. Am. Coll. Cardiol.* **73**, 2328–2344 (2019).
41. T. Kobayashi *et al.*, Molecular basis for gating of cardiac ryanodine receptor explains the mechanisms for gain- and loss-of function mutations. *Nat. Commun.* **13**, 2821 (2022).
42. N. Liu *et al.*, Abnormal propagation of calcium waves and ultrastructural remodeling in recessive catecholaminergic polymorphic ventricular tachycardia. *Circ. Res.* **113**, 142–152 (2013).
43. J. N. Weiss, A. Garfinkel, H. S. Karagueuzian, P. S. Chen, Z. Qu, Early afterdepolarizations and cardiac arrhythmias. *Heart Rhythm* **7**, 1891–1899 (2010).
44. Y. T. Zhao *et al.*, Arrhythmogenesis in a catecholaminergic polymorphic ventricular tachycardia mutation that depresses ryanodine receptor function. *Proc. Natl. Acad. Sci. U.S.A.* **112**, E1669–E1677 (2015).
45. S. Nattel, A. Maguy, S. Le Bouter, Y. H. Yeh, Arrhythmogenic ion-channel remodeling in the heart: Heart failure, myocardial infarction, and atrial fibrillation. *Physiol. Rev.* **87**, 425–456 (2007).
46. D. J. Tester, D. B. Spoon, H. H. Valdivia, J. C. Makielski, M. J. Ackerman, Targeted mutational analysis of the RyR2-encoded cardiac ryanodine receptor in sudden unexplained death: A molecular autopsy of 49 medical examiner/coroner's cases. *Mayo Clin. Proc.* **79**, 1380–1384 (2004).
47. R. D. Bagnall *et al.*, A prospective study of sudden cardiac death among children and young adults. *N. Engl. J. Med.* **374**, 2441–2452 (2016).